Nanoscale

Accepted Manuscript

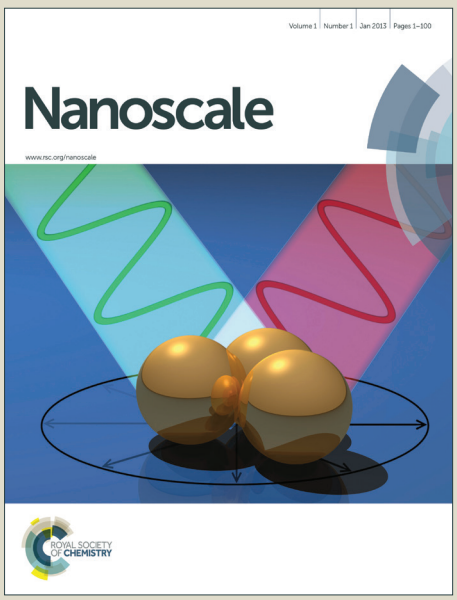

ROYAL SOCIETY OF CHEMISTRY

www.rsc.org/nanoscale

Cite this: DOI: 10.1039/c0xx00000x

www.rsc.org/xxxxxx

PAPER

Glutathione- and pH-Responsive Nonporous Silica Prodrug Nanoparticles for Controlled Release and Cancer Therapy

Zhigang Xu†, Shiying Liu†, Yuejun Kang,* and Mingfeng Wang*

Received (in XXX, XXX) Xth XXXXXXXXX 20XX, Accepted Xth XXXXXXXXX 20XX

DOI: 10.1039/b000000x

A myriad of drug delivery systems such as liposomes, micelles, polymers and inorganic nanoparticles (NPs) have been developed for cancer therapy. Very few of them, however, have the amenability of integrating multiple functionalities such as specific delivery, high circulation stability, controllable release and good biocompatibility and biodegradability in a single system to improve therapeutic efficacy. Herein, we report two types of stimuli-responsive nonporous silica prodrug NPs towards this goal for controlled release of anticancer drugs and efficient combinatorial cancer therapy. As a proof of concept, anticancer drugs camptothecin (CPT) and doxorubicin (DOX) were covalently encapsulated into silica matrices through glutathione (GSH)-responsive disulfide and pH-responsive hydrazone bonds, respectively, resulting in NPs with sizes tunable in the range of 50-200 nm. Both silica prodrug NPs showed stimuli-responsive controlled release upon exposure to GSH-rich or acidic environment, resulting in improved anticancer efficacy. Notably, two prodrug NPs simultaneously uptaken by HeLa cells showed remarkable combinatorial efficacy compared to free drug pairs. These results suggest that the stimuli-responsive silica prodrug NPs are promising anticancer drug carriers for efficient cancer therapy.

Introduction

Nanotechnology-based therapeutic platforms (also called nanomedicines) offer an opportunity to alter the pharmacokinetic profile of drugs, reduce off-target toxicity, and improve the therapeutic index.[1-4] A myriad of nanoscale drug delivery systems (DDSs), including liposomes, protein-drug conjugates, dendrimers, as well as polymeric and inorganic nanoparticles (NPs), have been developed for cancer therapy.[5-20] However, very few of previous DDSs have been translated into improved clinical outcomes. Some critical issues such as poor circulation stability, toxic side effects, low therapeutic efficacy, costly and tedious material synthesis and manufacturing still exist and limit the clinical applications of previous DDSs.[21-27] An ideal DDS is expected to show characteristics such as enhanced circulation stability, controlled release kinetics, good biocompatibility, and amenability for low-cost large-scale manufacturing.

Silica-based nanoscale drug carriers offer advantages such as highly controllable size, low toxicity, excellent biocompatibility, high stability in physiological conditions and sufficient biosafety for diagnostic and therapeutic applications.[28-30] Furthermore, the orthosilicic acid as the biodegradation product of silica NPs can be further absorbed by human bodies and efficiently excreted through the renal system.[31-33] In 2011, a class of ultrasmall nonporous silica NPs have been approved by US Food and Drug Administration (FDA) for clinical trials in cancer imaging.[30] Recent advances in synthetic technologies for rational size- and shape-tuning of silica NPs enable passive targeting to tumor cells and tissues through an enhanced permeability and retention (EPR) effect. Both mesoporous [34-42] and nonporous[43-48] silica NPs have been developed as carriers for drug or gene delivery. Compared to mesoporous silica NPs, nonporous analogues have shown better biosafety[49,50] and highly controllable size and shape.[28] In most of the previously reported nonporous silica drug NPs, drugs were either physically embedded into silica NPs or covalently linked with siloxane groups through degradable ester bonds.[43, 45, 46] However, some key features such as selective and controlled release of anticancer drugs and long-term stability were still lacking in these drug-silica NPs.

One of the most rational approaches of nanomedicine for cancer treatment is to develop stimuli-responsive nanoplatforms that integrate multiple functionalities such as specific delivery, controllable release and improved biocompatibility and biodegradability. For this purpose, some intrinsic features of tumor tissues can be exploited during the platform design. Tumor microenvironment is usually featured by low pH (between 6.0 and 7.0) compared to normal tissues and blood (~7.4), mainly because of high metabolic rate and rich level of CO_2. The pH value will decrease further from the extracellular microenvironment to intracellular organelles, such as endosomes (pH=5.5) and lysosomes (pH<5.5).[51, 52] Besides, tumor cells contain higher concentration of glutathione (GSH, 2–8 mM) than normal cells.[53, 54] These unique properties have been utilized to design stimuli-responsive nanoplatforms based on mesoporous silica[34, 39-41] and polymeric micelles [55-60] for drug delivery. Nevertheless, to the best of our knowledge, GSH- or pH-responsive DDS based on nonporous silica NPs, have not been reported so far.

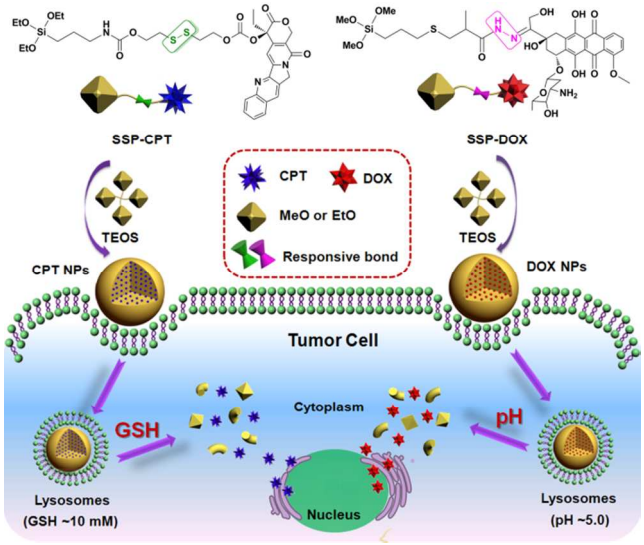

Figure 1. Schematic illustration of the chemical structures of silane-prodrug monomers (SSP-CPT and SSP-DOX); the formation of stimuli-responsive silica prodrug NPs *via* Stöber method using TEOS as the source of silane; illustrated mechanism of the endocytosis of NPs by tumor cells and the following GSH- and pH- induced drug release from the prodrug NPs.

Herein, we report two types of stimuli-responsive nonporous silica prodrug NPs by covalently linking anticancer drugs, namely camptothecin (CPT) and doxorubicin (DOX), to silica precursors through GSH- or pH-responsive bonds, respectively. These anticancer drug precursors were covalently encapsulated into the silica matrix through co-condensation with tetraethyl orthosilicate (TEOS) *via* the Stöber method.[61] While the covalent linkage between the anticancer drugs and the silica matrix is expected to minimize undesired leaching of the drugs during circulation in human body, the GSH- or pH-responsive chemical bonds (*i.e.* disulfide bond and hydrazine bond, respectively) enable stimuli-triggered drug release in tumors (Figure 1). Compared to previous drug delivery systems such as polymeric and mesoporous silica NPs, our nonporous silica prodrug NPs integrate features of easier synthesis, higher circulation stability, good biocompatibility and stimuli-responsive controlled release that are crucial for improving the drug efficacy in cancer therapy.

Results and discussion

We started from synthesis of two types of stimuli-responsive silane prodrug (SSP) monomers based on CPT and DOX, respectively, as two types of anticancer model drugs. Both CPT and DOX are commercially available and have been approved by US Food and Drug Administration (FDA) for cancer chemtherapy. CPT as a natural alkaloid shows high cytotoxic activity for various kinds of cancer cell lines;[62] while DOX is important for the treatment of tumours such as ovarian, gastric cancers and other kinds of cancers.[63] Specifically, commercial CPT molecules were covalently conjugated with triethoxysilane groups *via* a GSH-responsive disulfide bond to obtain SSP-CPT monomer (Figure S1-S3). Meanwhile, the DOX-conjugated monomer (SSP-DOX) with a trimethoxysilane group bearing a pH-responsive hydrazone bond was synthesized (Figure S4-S6). Details of synthesis and characterzation of these two SSP prodrug monomers are described in Supporting Information. Then the trialkoxysilane group of SSP drug monomers were hydrolyzed together with TEOS to form silica-prodrug NPs using Stöber method, which enables facile size control of NPs in the range of 50 ~ 200 nm by varying the concentrations of TEOS, water and ammonia, respectively, in methanol solution (Table S1,Table S2 and Figure S9). The resulting silica-prodrug NPs were denoted as CPT NPs (from SSP-CPT monomer) and DOX NPs (from SSP-DOX monomer), respectively. We also prepared dual-responsive and dual-drug NPs (Figure S10) by mixing two prodrug monomers of SSP-CPT and SSP-DOX into single NPs. However, the size, shape and the drug ratio of these NPs were less controllable compared to the NPs loaded with single prodrug. Therefore, the work herein mainly focused on the synthesis of NPs loaded with single prodrug, while allowing combinatorial co-delivery of both types of prodrug NPs for synergistic tumor treatment *in vitro*.

The UV−vis absorption spectra of both CPT and DOX NPs clearly show the successful incorporation of drug molecules into the prodrug NPs. As shown in Figure 2a-b, the aqueous solution of the prodrug NPs exhibited a characteristic absorption around 365 nm for CPT NPs and 490 nm for DOX NPs, but not in the control sample of pure silica NPs. The fluorescence emission spectra from both prodrug NPs (Figure 2c and d) were similar to

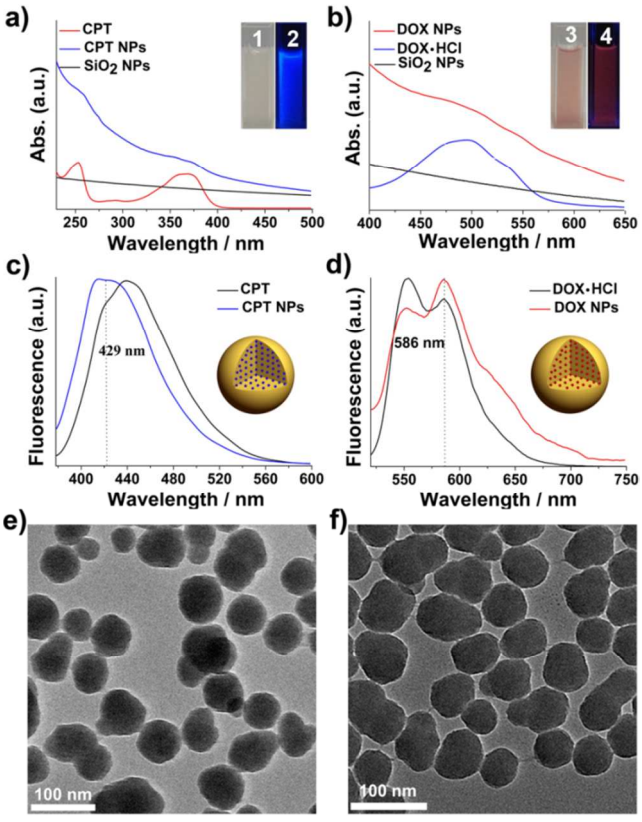

Figure 2. UV−vis absorption spectra of (a) SiO_2 NPs, CPT, CPT NPs and (b) SiO_2 NPs, DOX·HCl, DOX NPs in water. The insets of Figure a and b show digital photographs of the corresponding CPT NPs and DOX NPs dispersions in water under ambient light (Inset 1 and 3) and UV (365 nm) irradiation (Inset 2 and 4), respectively. The photoluminescence spectra of (c) CPT NPs and (d) DOX NPs in water. Excitation wavelength is 365 nm for CPT and 488 nm for DOX. TEM images of (e) CPT NPs and (f) DOX NPs.

those of the pristine drug molecules (CPT at 440 nm; DOX at 586 nm), except a slight blue shift of the maximal emission wavelength for CPT NPs *vs* pristine CPT and a relative enhancement of the red-edge emission of DOX NPs *vs* DOX·HCl. Moreover, the prodrug NPs in the aqueous dispersion show visible photoluminescence under UV light (365 nm) irradiation (Figure 2a-b, Inset 2 and 4), confirming the successful loading of drugs inside the prodrug NPs.

The morphology and the size of the silica prodrug NPs were characterized by transmission electron microscopy (TEM) and dynamic light scattering (DLS). Figure 2e-f show the representative TEM images of the silica prodrug NPs. These NPs appear spherical with an average diameter of 71.1 ± 12.9 nm for CPT NPs (Figure 2e) and of 67.1 ± 11.9 nm for DOX NPs (Figure 2f). Further measurement of the particle size using DLS (Figure S8) revealed an average hydrodynamic diameter of 112.1 nm (polydispersity index (PDI) = 0.121) for CPT NPs and 121.8 nm (PDI = 0.164) for DOX NPs. Such size difference between the TEM and the DLS measurements was also reported in other silica NPs.[39] Previous studies have shown that the size of therapeutic nanoplatform could affect the ability of deep tissue penetration and cancer cell internalization, and further impact the efficacy of nanomedicine.[64, 65] The average size of our silica-prodrug NPs is in the range of 50~100 nm, which is expected to avoid renal filtration during circulation in human body, thus increasing the circulation time of the drug carrier in the bloodstream and facilitating effective targeting of diseased tissues through the EPR effect.[31]

Because the drug molecules are chemically embedded into silica NPs, the drug leaching from these NPs under physiological environments is expected to be much lower compared to previously reported silica NPs containing physically trapped drugs.[44] To evaluate this hypothesis, we first studied the controlled release from CPT NPs in phosphate buffered saline (1×PBS, pH 7.4) at 37 °C with or without GSH, resembling the difference of cellular environment between tumor cells and normal cells. Figure 3a shows that the drug release in the PBS buffer containing 10 mM GSH was significantly faster than that in the same buffer without GSH. Specifically, approximately 65.5 % of CPT was released from CPT NPs in 120 h in the presence of 10 mM of GSH. In contrast, only 6.0 % of CPT was released in the absence of GSH while other conditions were the same. Then we also studied the controlled release of DOX NPs in 1×PBS buffers at 37 °C with different pH values, *i.e.* pH 7.4 and 5.0, respectively. Figure 3a shows that the release of DOX under mildly acidic environment was significantly faster than that in neutral environment because of the pH-sensitivity of the hydrazone bond. Similar to CPT NPs, approximately 71.5 % of DOX was released from NPs in 120 h at pH 5.0, whereas only about 10.0 % DOX was released at pH 7.4.

To better understand the mechanism of the controlled drug release from the silica prodrug NPs, we further studied the morphological change of the silica prodrug NPs under various conditions. The CPT or DOX NPs were firstly incubated in 1×PBS buffer (pH 7.4), and the TEM images showed no

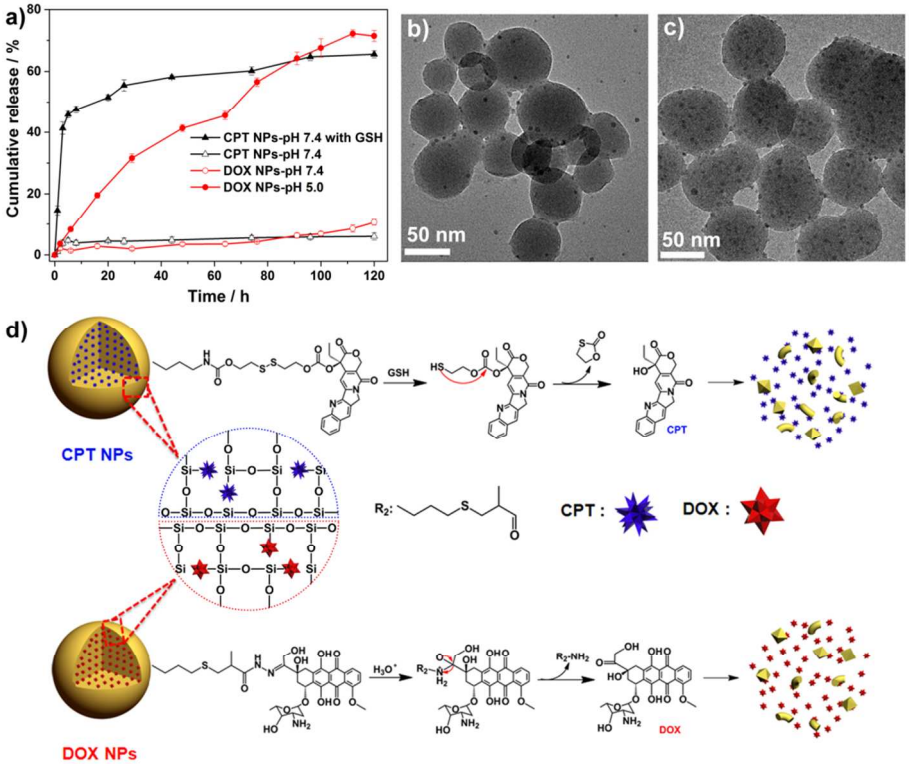

Figure 3. (a) *In vitro* release profiles of CPT from the CPT NPs in PBS (pH 7.4) at 37 °C with or without GSH treatment and DOX from DOX NPs in PBS at pH 7.4 and 5.0 at 37 °C. Data were shown as the means ± SD (n=3). (b) TEM image of CPT NPs after being incubated in PBS (50 mM, pH 7.4) containing 10 mM GSH for 72 h; (c) TEM image of DOX NPs after being incubated in PBS (50 mM, pH 5.0) for 72 h. (d) Proposed degradation and stimuli induced-release mechanism of CPT or DOX from the CPT NPs or DOX NPs, respectively.

significant change even after 120 h (Figure S12). Different results were observed when these prodrug NPs were exposed to their corresponding stimuli agents, *i.e.* GSH for CPT NPs and acidic species for DOX NPs. Specifically, there are some even smaller daughter particles with an average diameter ~4 nm appeared on the surfaces of CPT NPs incubated in in 1×PBS (pH 7.4, 10 mM GSH) over 72 h (Figure 3b). Similar phenomena were observed in DOX NPs incubated in 1×PBS (pH 5.0) (Figure 3c). We note that more significant degradation of both CPT and DOX NPs was observed under TEM when the incubation time increased to 120 h (Figure S13).

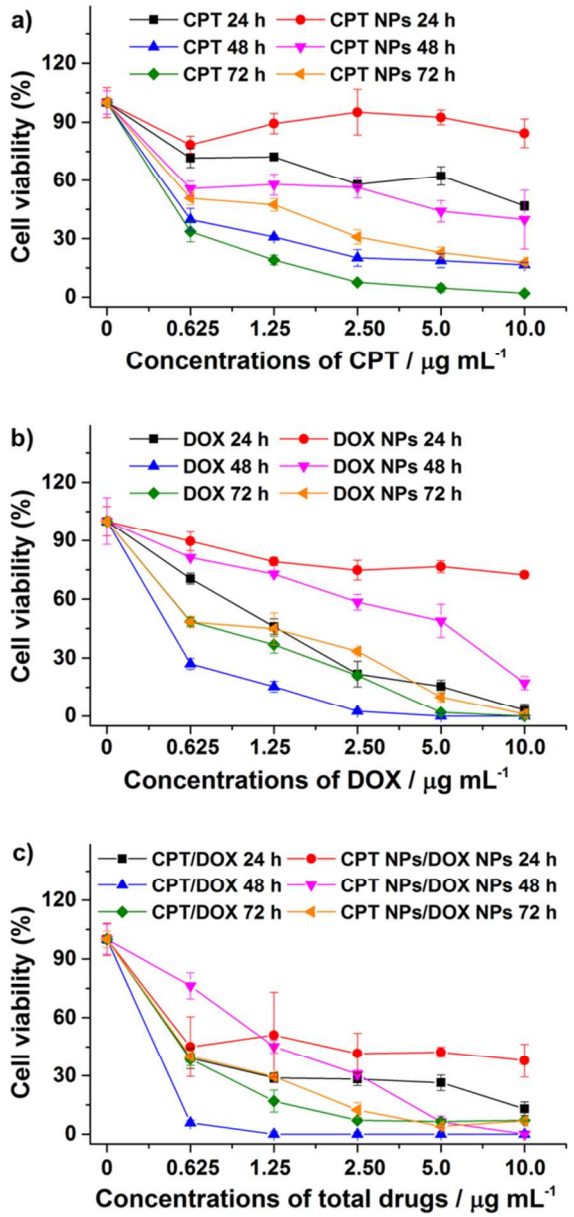

Figure 4. Cell viability of HeLa cells after treatment with different concentrations of (a) free CPT and CPT NPs, (b) free DOX and DOX NPs, and (c) co-delivery of both drugs for 24 h, 48 h, and 72 h tested by PrestoBlue assay. The mass ratio of free drug or prodrug NPs is 1:1 for co-delivery. Cells without treatment were used as control. Data were shown as means ± SD (n=3).

In contrast, such daughter particles were not observed in blank silica NPs incubated in PBS buffer solution containing 10 mM GSH (pH 7.4) (Figure S14). We speculate that these daughter particles were due to the release of drug molecules from inside of the prodrug NPs. These results suggest that the prodrug NPs are relatively stable under physiological conditions in the absence of stimuli, which is important to reduce the side effects caused by non-specific leaching of anticancer drugs from the carriers.

The GSH- and pH-responsive release of drug molecules from the silica prodrug NPs as described above should be attributed to the cleavage of disulfide and hydrazine bonds, respectively. A proposed mechanism of the controlled release is presented in Figure 3d. The scission of disulfide bonds is expected to be followed by intramolecular cyclization and cleavage of neighboring carbamate bond,[66, 67] resulting in release of native CPT molecules from the matrix of silica NPs. Similar to CPT NPs, DOX NPs were relatively stable under physiological conditions but quickly responded to acidic conditions equivalent to the endo/lysosomal environment. In an acidic environment at pH 5.0, hydrazine bonds are cleaved resulting in the release of native DOX molecules. The slow release of DOX from the NPs suggests that the sillica matrix serves as a physical barrier to retard the diffusion of acid into the NPs and the diffusion of cleaved DOX out from the NPs.[51]

To demonstrate the *in vitro* cytotoxicity of two types of prodrug NPs, we used HeLa cells (a derived cell line from cervical cancer) as a model. When the incubation time increased from 24 to 72 h, treatment with CPT NPs reduced the viability of HeLa cells significantly (Figure 4a). Given that blank silica NPs caused little toxicity in HeLa cells (Figure S15), the viability reduction was attributed mainly to the released CPT under high GSH level in tumor cells, which induced breakage of the disulfide linker. After 72 h, CPT NPs (10 μg mL^{-1}) could kill more than 80% of cancer cells. Furthermore, DOX NPs exhibited similar anticancer effects as shown in Figure 4b. More DOX were released from the DOX NPs during prolonged incubation due to the relatively low pH in tumor cell microenvironment, leading to a higher level of cell death. After 72 h, less than 5% of HeLa cells remained alive after being treated with DOX NPs. It should be noted that the cell viability after treatment with free DOX over 72 h was even higher than that after 48 h, which might indicate that some survived HeLa cells had developed drug resistance against DOX and continued to proliferate to 72 h. Nevertheless, such drug resistance was not observed in the cells treated by DOX NPs.

Table 1 Combination index (CI)[a] value for free drug and prodrug NPs-100 of different time.

Sample	CI (24 h)	CI (48 h)	CI (72 h)
Free drug (CPT and DOX)	0.24	0.70	0.95
Prodrug NPs (CPT NPs and DOX NPs)	< 0.11	0.28	0.85

[a] when CI < 1, indicating a synergistic effect; CI = 1, indicating an additive effect; CI > 1, indicating an antagonism effect.

To further investigate the combined therapeutic effect resulted from both CPT and DOX, we also studied the co-delivery of free drugs and silica prodrug NPs over different

incubation periods. Generally, free drugs are transported by passive diffusion through cell membranes, while the silica prodrug NPs enters the cells *via* endocytosis. The endocytosis usually shows a slower transportation rate than passive diffusion, thus resulting in relatively lower cytotoxicity of prodrug NPs in early stage of incubation. In Figure 4c, the co-delivery of two prodrug NPs exhibited a higher cytotoxicity than application of single prodrug NPs, indicating the advantage of combinatorial delivery of multiple drugs. Additionally, this co-delivery strategy was evaluated using the combination index (CI) theorem of Chou-Talalay based on the IC_{50} value of drugs (Table S3).[68] According to Chou-Talalay method, CI < 1 indicates a synergistic effect; CI = 1 indicates an additive effect; while CI >1 indicates an antagonism effect. As shown in Table 1, the CI of all drug combinations, free or prodrug NPs, were all lower than 1, indicating a synergistic effect of combining CPT and DOX for supression of tumor cells. In addition, the prodrug NPs pairs showed a significantly lower CI than free drug pairs, further promoting the drug efficacy. Compared to the previously reported co-delivery modality by encapsulating both CPT and DOX in single silica or polymeric NPs,[69-73] our approach shows better capability in controlling the mass ratio of multiple drugs by optimal combination of different prodrug NPs.[74]

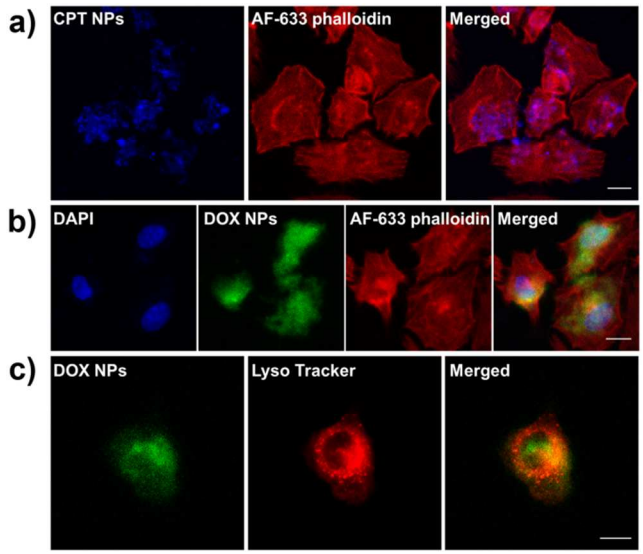

Figure 5. Cellular internalization and co-localization analysis of HeLa cells after treatment with CPT NPs and DOX NPs for desired time. (a) Cellular uptake of CPT NPs in HeLa cells after 20 h. The fluorescence of CPT NPs and Alexa Fluor® 633 phalloidin were pseudo-labeled as blue and red, respectively. (b) Cellular uptake of DOX NPs in HeLa cells after 20 h. The fluorescences of DAPI, DOX NPs, and Alexa Fluor® 633 phalloidin were pseudo-labeled with blue, green, and red, respectively. (c) Co-localization analysis of lysosome of HeLa cells and DOX NPs after incubation for 5 h, the fluorescences of DOX NPs and Lyso Tracker were pseudo-labeled with green and red, respectively. Scale bars: 20 μm.

In order to characterize the intracellular localization of the prodrug NPs in HeLa cells, confocal laser scanning microscopy was used to visualize the NPs in the cellular context labelled with a few commercial organic dyes. Figure 5a shows the fluorescence of CPT NPs (blue) and Alexa Fluor® 633 phalloidin (red for cytoskeleton). The merged image and ortho views of different z-stack (Figure S16a) prove that CPT NPs can be uptaken by the HeLa cells into the cytoplasm. Figure 5b indicates the fluorescence of DAPI (blue for neuclei), DOX NPs (green), and Alexa Fluor® 633 phalloidin (red for cytoskeleton) in HeLa cells. The co-localization of DAPI and DOX NP in Figure 5b and the ortho views (Figure S16b) suggest that DOX NPs not only can be internalized by HeLa cells into cytoplasm but also can enter the nucleus, which may further enhance the cytotoxic effect of DOX. In addition, by labeling lysosome in HeLa cells with Lyso Tracker, we found that DOX NPs (green) appeared to co-localize with lysosome (red) and the merged region appears yellow (Figure 5c). This finding revealed that most of the uptaken DOX NPs were located in lysosomes, where the local pH was lower and hence promoted the DOX release against tumor cells.[51]

The cellular uptake of CPT NPs and DOX NPs were further verified by flow cytometry analysis. The fluorescence intensity of single cell emission measured by flow cytometry can be a good indication of the amount of NPs internalized by each cell. As shown in Figure 6a and 6c, the peak of fluorescence intensity shifted to a higher level when increasing the incubation time with NPs, suggesting the promoted NP internalization by HeLa cells. The percentage of cells that had uptaken significant amount of CPT NPs increased from 59.9 % in 4 h to 92.8 % in 48 h, indicating the impressive efficiency of drug delivery. The cellular uptake of DOX NPs showed a similar trend (Figure 6b and 6d) with cellular uptake percentage rising notably from 50.7 % in 4 h to 98.2 % in 48 h. Therefore, the previously observed higher cytotoxicity of these prodrug NPs after 48 h can be attributed to the high cellular uptake ratio.

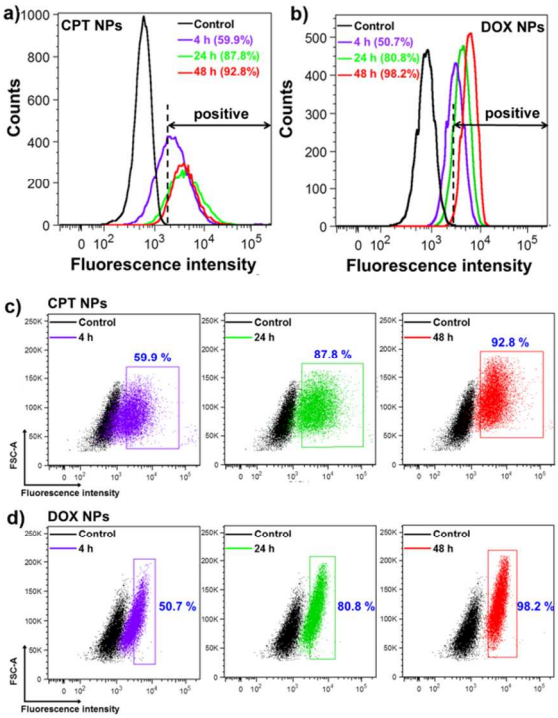

Figure 6. Flow cytometry analysis of cellular uptake of (a) CPT NPs and (b) DOX NPs in HeLa cells after different incubation time. The control represents the unlabelled cells. Corresponding flow cytometry dot plots of HeLa cells after treatment with (c) CPT NPs and (d) DOX NPs for different time.

Conclusions

We have developed two types of nonporous silica prodrug

NPs that encapsulate anticancer drugs (*e.g.* CPT and DOX) through GSH- or pH-responsive chemical bonds, respectively. Both silica prodrug NPs prepared through the Stöber method showed relatively good stability under normal physiological conditions. Dramatically enhanced release of the entrapped anticancer drugs was observed upon exposure of these prodrug NPs to GSH-rich or acidic conditions similar to the cellular microenvironment of cancer cells. *In vitro* drug release studies indicated that the prodrug NPs effectively inhibited the proliferation of cancer cells and showed impressive anticancer efficacy. Moreover, the combined cancer chemotherapy using both CPT and DOX delivered by the silica prodrug NPs was studied, indicating a promising combinatorial therapeutic effect. Further development based on this stimuli-responsive silica prodrug platform is feasible by integrating multiple functional components, such as imaging and therapeutic agents, to achieve the long-term goal of personalized nanomedicines for future healthcare.

Experimental section

Materials

All chemical reagents including tetraethyl orthosilicate (TEOS, 99.99 %), Glutathione (GSH, 98 %), bis(2-hydroxyethyl) disulfide (BHD, technical grade), triphosgene (BTC, 98 %), 4-(Dimethylamino)pyridine (DMAP, 99 %), dibutyltin dilaurate (DBTDL, 95 %), tert-Butyl carbazate (BH, 98 %), trifluoroacetic acid (TFA, 99 %), triethylamine (TEA, 99 %), (3-mercaptopropyl) trimethoxysilane, 3-(triethoxysilyl)propyl isocyanate 4',6-diamidino-2-phenylindole (DAPI), bovine serum albumin (BSA) and formalin solution were provided by Sigma-Aldrich (USA) and used as received unless otherwise noted. Methacryloyl chloride (MA, 98 %) was purchased from Alfa Aesar and used as received. Camptothecin(CPT) was supplied by Chengdu labooo Plant and chemical CO. Ltd (Chengdu, China). Doxorubicin hydrochloride (DOX·HCl) was obtained from Beijing HuaFeng United Technology CO. Ltd (Beijing, China). All anhydrous solvents including methanol (CH_3OH), acetonitrile (CH_3CN), tetrahydrofuran (THF), methylene chloride (DCM), dimethyl sulfoxide (DMSO) and chloroform (CH_3Cl_3) were also provided by sigma-aldrich (USA) and used directly. All the other solvents were analytical grade and provided by the Ctech Global Pte Ltd (Singapore). Dulbecco's Modified Eagle's Medium (DMEM), fetal bovine serum (FBS), penicillin /streptomycin mixture, phosphate buffered saline (PBS), Alexa Fluor® 633 phalloidin, TrypLE™ Express Enzyme (1×), Lyso Tracker® Red DND-99 and PrestoBlue cell viability reagent were purchased from Life Technologies (Singapore). Deionized (D.I.) water was prepared from Millipore (Bedford, MA, USA).

Characterization

^{1}H NMR spectra were recorded on a Bruker AV 300 or 400 NMR spectrometer (Rheinstetten, Germany) using tetramethylsilane as an internal standard at 25 ℃ .The size distribution and ζ-potentials of all prodrug NPs were determined by dynamic light scattering (DLS) using a BI-200SM (Brookhaven, USA) with angle detection at 90°. The morphology of the samples was recorded by an energy filtered Carl Zeiss transmission electron microscopy (TEM), LIBAR®120 with in-column Omega spectrometer (Germany) or Scanning Electron Microscope (SEM, JEOL JSM-6700F, Japan), and samples for TEM or SEM measurements were made by casting one drop of the sample's solution on carbon-coated copper grids and on silicon wafer, respectively. The Fourier transform infrared (FTIR) spectra were acquired on a Perkin Elmer FTIR spectrophotometer (USA) using KBr pellets. Fluorescence spectra were recorded on a Perkim Elmer LS-55 fluorescence spectrometer (Perkim Elmer, USA). Absorbance spectra were carried out using a Shimadzu Uv-2450 visible spectrophotometer (Shimadzu, Japan). The fluorescence images of cells were taken using a confocal laser scanning microscopy (LSM 780, Carl Zeiss, Germany).

General Method of Preparing 100 nm-Sized Prodrug Nanoparticles (NPs)

The prodrug NPs were synthesized using a modified Stöber method.[61] Typically, 60 mg of tetraethyl orthosilicate (TEOS) were dissolved in a 1.0 mL methanol and 0.11 mL of ammonia and 0.36 mL of water, then a DMSO solution (30 μL) of SSP-CPT or SSP-DOX (2.0 mg) was added. After 12 hours of stirring, the resulting prodrug NPs were isolated by centrifugation at the speed of 14000 rpm, and the supernatant was removed. The isolated products were dispersed in ethanol. The washing and dispersion was repeated 3 times. Finally, the prodrug NPs solution was centrifuged at the speed of 3000 rpm to remove any aggregated particles. The purified prodrug NPs were homogeneously dispersed in 2 mL ethanol and denoted as CPT NPs-100 or DOX NPs-100, respectively. The blank SiO_2 NPs-100 was prepared using a same method without SSP-drug additive, which used as a control experiment. The size and shape of the prodrug NPs were characterized by TEM, SEM or DLS, respectively. Synthetic procedures were similar for 50 or 200 nm-sized silica prodrug NPs except the amount of water and ammonia. Table S1 summarizes the synthesis conditions for silica prodrug NPs of various sizes.

Drug Loading and Drug Release *In Vitro*

To determine the drug content in silica prodrug NPs. Typically, 1 mL of the prodrug NPs (CPT NPs-50, 100 or 200; DOX NPs-50, 100 or 200) ethanol solution was centrifuged at 14000 rpm for 10 min, and the resulting prodrug NPs solid were completely dissolved in 10 mL KOH (1.0 M) for 2 h, followed by adding 10 mL HCl (1.0 M) for neutralizing. The suspension was centrifuged for 10 min at 14000 rpm and the upper clear solutions were collected. Then the amount of free CPT or DOX was calculated based on a calibration curve by UV−visible spectroscopy with absorption spectrum at 365 or 488 nm. All the experiments were carried out in triplicate. The loading content (LC %) of CPT or DOX was calculated by the equation: [54]

$$\text{LC \%} = \frac{\text{amount of drug in nanoparticles}}{\text{amount of nanoparticles}} \times 100\%$$

The release of drug from prodrug NPs was evaluated by the following method. Typically, 0.5 mL of the prodrug NPs (CPT NPs-100 or DOX NPs-100) ethanol solutions were centrifuged at 14000 rpm for 10 min, and the resulting prodrug NPs solid was dispersed in 15 mL phosphate buffered saline (1×PBS, pH 7.4) with or without 10 mM GSH for CPT NPs and different pH

values (*i.e.* pH 7.4 or 5.0) for DOX NPs. The suspension solutions of prodrug NPs were equally distributed to 15 vials with 1 mL of silica prodrug NPs solution and then incubated at 37 °C. One selected vial of each group was taken out at different time points from the incubator and centrifuged at 14 000 rpm for 10 min. The supernatant (1 mL) was transferred to a glass bottle and diluted with 2 mL of corresponding buffer solutions, and the resulting solution was measured by fluorescence spectroscopy. The release amount of CPT or DOX was calculated based on a calibration curve (As shown in Figure S11) by fluorescence spectroscopy with an excitation spectrum at 365 or 488 nm. Above release experiments were tested in triplicate.

Cell Culture

HeLa cell line was obtained from ATCC and cultured in DMEM (Dulbecco's Modified Eagle's Medium) with 10 % (vol/vol) fetal bovine serum (FBS) and 1 % penicillin /streptomycin mixture at 37 °C with 5 % CO_2.

***In Vitro* Cytotoxicity**

PrestBlue assay was performed to test the cell viability, in which a nonfluorescent blue compound called resazurin ($\lambda_{max.abs}$ = 600 nm) in PrestoBlue® reagent can be reduced by live cells to resorufin ($\lambda_{max.abs}$ = 570 nm) exhibiting strong red fluorescence. By measuring the absorbance at 570 and 600 nm, cell viability can be calculated relative to the control cells without drug treatment. The cytotoxicity of free CPT, free DOX, CPT NPs-100, DOX NPs-100 and blank silica NPs in HeLa cells was studied by the following method. Firstly, HeLa cells were seeded on a 96-well plate (10000 cells per well) and cultured at 37 °C with 5 % CO_2. After 12 h for attachment, the culture medium was replaced with fresh medium containing blank silica NPs with a varied concentrations ranging 38.6 to 617.0 μg mL^{-1} and for free drug and prodrug NPs with a varied concentrations ranging 0.625 to 10.0 μg mL^{-1} for 24 h, 48 h and 72 h, respectively. Then the culture medium was removed and cells were washed three times by 1×PBS to remove excess NPs. Then, PrestoBlue reagent diluted by DMEM were added to each wells and incubated at 37 °C with 5 % CO_2. At the same time, PrestoBlue® reagents diluted by DMEM were also added to blank wells without cells as control. After 1 h incubation, the absorbance at 570 nm (reference wavelength is 600 nm) was detected by Plate Reader (Tecan Infinite M200 series Pro, Tecan Asia, Singapore). All samples were tested in triplicates. Cells without treatment by NPs were used as control and corresponding cell viability was set as 100 %. Data were analyzed according to the protocol.

***In Vitro* Cellular Uptake by Confocal Laser Scanning Microscopy (CLSM)**

HeLa cells were seeded on a 6-well plate and cultured in 37 °C with 5 % CO_2. After 12 h for attachment, CPT NPs-100 and DOX NPs-100 (CPT final concentration: 5 μg mL^{-1}, DOX final concentration: 50 μg mL^{-1}) were added to the medium and incubated with HeLa cells at 37 °C with 5 % CO_2. After 20 h, excess NPs were washed with 1×PBS for five times. After that, cells were fixed by formalin solution for 20 min and then washed by 1×PBS extensively for three times. Then cells were permeabilized with 0.1 % (vol/vol) Triton X-100 in 1×PBS for 5 minutes at room temperature. After washing twice by 1×PBS, cells were blocked for 30 min in 1×PBS containing 1 % (wt/vol) BSA. Then Alexa Fluor® 633 phalloidin in 1×PBS was added to stain filamentous actin (F-actin) cytoskeleton for 1 h at room temperature. After washing three times, nucleus of cells samples in DOX NPs-100 group was stained by DAPI for 1 min at room temperature and then samples were washed three times and then added in fresh 1×PBS. Lasers of 405, 488, and 633 nm were used to excite DAPI, DOX NPs-100, and Alexa Fluor® 633 phalloidin, respectively. The corresponding fluorescence emissions were recorded by a confocal laser scanning microscopy (LSM 780, Carl Zeiss, Germany) using a band-pass filter combination including 410-481 nm, 490-630 nm, and 638-747 nm for imaging in three individual channels (Objective: LD Plan-Neofluar 20x/0.4 Korr M27). However, the cells in CPT NPs-100 were not stained by DAPI. Lasers of 405 and 633 nm were used to excite CPT NPs-100 and Alexa Fluor® 633 phalloidin, respectively. The corresponding fluorescence emissions were recorded by LSM 780 with 410-481 nm and 638-747 nm for imaging in the two channels (Objective: LD Plan-Neofluar 20x/0.4 Korr M27).

Lysosome Colocalization by CLSM. HeLa cells were seeded on a 6-well plate and cultured at 37 °C with 5 % CO_2. After 12 h for attachment, DOX NPs-100 (DOX final concentration: 50 μg mL-1) were added to the medium and incubated with HeLa cells at 37 °C with 5 % CO_2. After 5 h, excess NPs were washed with 1×PBS for five times. Thereafter, Lyso Tracker® Red DND-99 diluted in DMEM (10 μM) were added to the cells and incubated for 30 min. Then the cells samples were washed by 1×PBS twice and exposed to CLSM for observation. Lasers of 488 and 561 nm were used to excite DOX NPs-100 and Lyso Tracker® Red DND-99, respectively. The corresponding fluorescence emissions were recorded by LSM 780 with 493-555 nm and 566-670 nm for imaging in the two channels (Objective: LD Plan-Neofluar 20x/0.4 Korr M27).

***In Vitro* Cellular Uptake by Flow Cytometry**

HeLa cells were seeded on a 6-well plate and cultured in 37 °C with 5% CO_2. After 12 h for attachment, CPT NPs-100 and DOX NPs-100 (CPT final concentration: 2 μg mL^{-1}, DOX final concentration: 10 μg mL^{-1}) were added to the medium and incubated with HeLa cells at 37 °C with 5 % CO_2 for 4 h, 24 h, and 48 h. After desired time, excess NPs were washed by 1×PBS extensively for three times. Then the cells were detached by TrypLE Express and then the culture medium was added to stop trypsinization. After centrifugation, the supernatant were thrown away and 1×PBS (500 μL) were added to resuspend the cells for flow cytometry (LSRII, BD Biosciences). The fluorescence of CPT NPs-100 and DOX NPs-100 were detected using DAPI (excitation: 355 nm, emission: 385 nm-425 nm) and FITC (excitation: 488 nm, emission: 500 nm-560 nm) channels, respectively with around 10000 gated cells. The cells without any fluorescence labeling were used as control. The flow cytometry data were analyzed using FlowJo software.

The Combinatorial Therapeutic Effect of Free Drug and Prodrug NPs

To investigate the combinatorial therapeutic effect resulted from co-delivery of CPT and DOX anticancer drugs, we studied the co-delivery of free drugs and prodrug NPs under different time durations and measured the corresponding cell viability after

treatment (Figure 4 and Table S3). Combination index (CI) was used to show the combined effects of drugs, and the CI value was calculated on the basis of the Equation:

$$CI = \frac{IC_{50}(A)_{Pair}}{IC_{50}(A)} + \frac{IC_{50}(A)_{Pair}}{IC_{50}(B)}$$

Where IC_{50} is the drug concentration that makes the cell viability at 50 %, the IC_{50}(A) and the IC_{50}(B) are the IC_{50} value with the drug given individually, and the $IC_{50}(A)_{pair}$ and the $IC_{50}(B)_{pair}$ are the IC_{50} value with the drug given as A-B pair.

Acknowledgements

M.W. is grateful to the funding support by a start-up grant from Nanyang Technological University, and AcRF Tier 2 (ARC 36/13) from the Ministry of Education, Singapore. Y.K. acknowledges the AcRF Tier 2 (ARC 22/13) from the Ministry of Education, Singapore.

Notes and references

† *These authors contributed equally to this work.*

School of Chemical and Biomedical Engineering, Nanyang Technological University, 62 Nanyang Drive, Singapore 637459, Singapore

[b] *Address, Address, Town, Country. Fax: +65 63168746; Tel: +65 6794 7553; E-mail: yuejun.kang@ntu.edu.sg; mfwang@ntu.edu.sg.*

† Electronic Supplementary Information (ESI) available: Experimental details of SSP-CPT and SSP-DOX; ^{1}H NMR and FT-IR spectra; DLS, TEM and SEM images of prodrug NPs; TEM image, UV-vis absorption and photoluminescence spectra of CPT/DOX NPs; the TEM images of prodrug NPs incubated with physiological conditions; the reaction conditions and structure information of size-controlled prodrug NPs; IC_{50} value of free drug and prodrug NPs of different time. See DOI: 10.1039/b000000x/.

1. S. Mura, J. Nicolas, P. Couvreur, *Nat. Mater.*, 2013, **12**, 991-1003.
2. V. P. Chauhan, R. K. Jain, *Nat. Mater.,* 2013, **12**, 958-962.
3. K. Riehemann, S. W. Schneider, T. A. Luger, B. Godin, M. Ferrari, H. Fuchs, *Angew. Chem. Int. Ed.,* 2009, **48**, 872-987.
4. Z. Cheng, A. A. Zaki, J. Z. Hui, V. R. Muzykantov, A. Tsourkas, *Science*, 2012, **338**, 903-910.
5. Z. Yang, J. H. Lee, H. M. Jeon, J. H. Han, N. Park, Y. He, H. Lee, K. Hong, C. Kang, J. S. Kim, *J. Am. Chem. Soc.*, 2013, **135**, 11657-11662.
6. X. Wu, X. Sun, Z. Guo, J. Tang, Y. Shen, T. D. James, W. Zhu, *J. Am. Chem. Soc.*, 2014, **136**, 3579-3588.
7. W. Cao, Y. Gu, M. Meineck, T. Li, H. Xu, *J. Am. Chem. Soc*., 2014, **136**, 5132-5137.
8. X. Hu, J. Hu, J. Tian, Z. Ge, G. Zhang, K. Luo, S. Liu, *J. Am. Chem. Soc.,* 2013, **135**, 17617-17619.
9. Z. Luo, X. Ding, Y. Hu, S. Wu, Y. Xiang, Y. Zeng, B. Zhang, H. Yan, H. Zhang, L. Zhu, J. Liu, J. Li, K. Cai, Y. Zhao, *ACS Nano*, 2013, **7**, 10271-10284.
10. S. Li, K. Hu, W. Cao, Y. Sun, W. Sheng, F. Li, Y. Wu, X. J. Liang, *Nanoscale*, 2014, **6**, 13701-13709.
11. G. Mikhaylov, D. Klimpel, N. Schaschke, U. Mikac, M. Vizovisek, M. Fonovic, V. Turk, B. Turk, O. Vasiljeva, *Angew. Chem. Int. Ed.,* 2014, **53**, 10077-10081.
12. J. Tian, L. Ding, H. Ju, Y. Yang, X. Li, Z. Shen, Z. Zhu, J. Yu, C. A Yang, *Angew. Chem. Int. Ed.,* 2014, **53**, 9544-9549.
13. F. Kievit, M. Zhang, *Adv. Mater.*, 2011, **23**, H217-H247.
14. T. Sun, Y. Zhang, B. Pang, D. Hyun, M. Yang, Y. Xia, *Angew. Chem. Int. Ed*., 2014, **53**, 12320-12364.
15. Y. Kakizawa, K. Kataoka, *Adv. Drug Deli. Rev.,* 2002, **54**, 203-222.
16. J. Park, S. Lee, J. Kim, K. Park, K. Kim, I. Kwon, *Prog. Polym. Sci.,* 2008, **33**, 113-137.
17. O. Farokhzad, R. Langer, *ACS Nano*, 2009, **3**, 16-20.
18. V. Delplace, P. Couvreur, J. Nicolas, *Polym. Chem.*, 2014, **5**, 1529-1544.
19. N. Kamaly, Z. Xiao, P. M. Valencia, A. F. Radovic-Moreno, O. C. Farokhzad, *Chem. Soc. Rev.*, 2012, **41**, 2971-3010.
20. L. Gros, H. Ringsdorf, H. Schupp, *Angew. Chem. Int. Ed.,* 1981, **20**, 305-325.
21. S. Yu, J. Ding, C. He, Y. Cao, W. Xu, X. Chen, *Adv. Healthcare. Mater.*, 2014, **3**, 752-760.
22. E. Chow, D. Ho, *Sci. Transl. Med.*, 2013, **5**, 216rv4.
23. Y. Wang, M. S. Shim, N. S. Levinson, H.-W. Sung, Y. Xia, *Adv. Funct. Mater.*, 2014, **24**, 4206-4220.
24. S. Bonacchi, D. Genovese, R. Juris, M. Montalti, L. Prodi, E. Rampazzo, N. Zaccheroni, *Angew. Chem. Int. Ed.*, 2011, **50**, 4056-4066.
25. M. Montalti, L. Prodi, E. Rampazzo, N. Zaccheroni, *Chem. Soc. Rev*., 2014, **43**, 4243-4268.
26. J. Nicolas, S. Mura, D. Brambilla, N. Mackiewicz, P. Couvreur, *Chem. Soc. Rev.*, 2013, **42**, 1147-1235.
27. S. Swaminathan, J. Amoros, A. Fraix, N. Kandoth, S. Sortino, F. M. Raymo, *Chem. Soc. Rev.,* 2014, **43**, 4167-4178.
28. L. Tang, J. Cheng, *Nano today*, 2013, **8**, 290-312.
29. A. Bumb, S. Sarkar, N. Billington, M. Brechbiel, K. Neuman, *J. Am. Chem. Soc.*, 2013, **135**, 7815-7818.
30. R. Friedman, *J. Natl. Cancer I.,* 2011, **103**, 1428-1429.
31. J. Park, L. Gu, G. von Maltzahn, E. Ruoslahti, S. Bhatia, M. Sailor, *Nat. Mater*., 2009, **8**, 331-336.
32. X. He, H. Nie, K. Wang, W. Tan, X. Wu, P. Zhang, *Anal. Chem.*, 2008, **80**, 9597-9603.
33. R. Kumar, I. Roy, T. Ohulchanskky, L. Vathy, E. Bergey, M. Sajjad, P. Prasad, *ACS Nano*, 2010, **4**, 699-708.
34. D. Tarn, C. Ashley, M. Xue, E. Carnes, J. Zink, C. Brinker, *Acc. Chem. Res*., 2013, **46**, 792-801.
35. J. E. Lee, N. Lee, T. Kim, J. Kim, T. Hyeon, *Acc. Chem. Res.,* 2011, **44**, 893-902.
36. C. Coll, A. Bernardos, R. Martínez-Máñez, F. Sancenón, *Acc. Chem. Res.*, 2012, **46**, 339-349.
37. P. Yang, S. Gai, J. Lin, *Chem. Soc. Rev.*, 2012, **41**, 3679-3698.
38. H. Meng, W. X. Mai, H. Zhang, M. Xue, T. Xia, S. Lin, X. Wang, Y. Zhao, Z. Ji, J. I. Zink, A. E. Nel, *ACS Nano*, 2013, **6**, 994-1005.
39. Z. Luo, K. Cai, Y. Hu, L. Zhao, P. Liu, L. Duan, W. Yang, *Angew. Chem. Int. Ed.,* 2011, **50**, 640-643.
40. Z. Luo, X. Ding, Y. Hu, S. Wu, Y. Xiang, Y. Zeng, B. Zhang, H. Yan, H. Zhang, L. Zhu, J. Liu, H. Li, K. Cai, Y. Zhao, *ACS Nano*, 2013, **7**, 10271-10284.
41. C. H. Lee, S. H. Cheng, I. P. Huang, J. S. Souris, C. S. Yang, C. Y. Mou, L. W. Lo, *Angew. Chem. Int. Ed.,* 2010, **49**, 8214-8219.
42. Q. J. He, Y. Gao, L. X. Zhang, Z. W. Zhang, F. Gao, X. F. Ji, Y. P. Li, J. L. Shi, *Biomaterials*, 2011, **32**, 7711-7720.
43. L. Tang, X. Yang, L. Dobrucki, I. Chaudhury, Q. Yin, C. Yao, S. Lezmi, W. Helferich, T. Fan, J. Cheng, *Angew. Chem. Int. Ed.,* 2012, **51**, 12721-12726.
44. S. Zhang, Z. Chu, C. Yin, C. Zhang, G. Lin, Q. Li, *J. Am. Chem. Soc.,* 2013, **135,** 5709-5716.
45. L. Tang, T. Fan, L. Borst, J. Cheng, *ACS Nano*, 2012, **6**, 3954-3966.
46. L. Tang, N. P. Gabrielson, F. Uckun, T. Fan, J. Cheng, *J. Mol. Pharm.*, 2013, **10**, 883-892.
47. Y. Chen, Y. Gao, H. Chen, D. Zeng, Y. Li, Y. Zheng, F. Li, X. Ji, X. Wang, F. Chen, Q. He, L. Zhang, J. Shi, *Adv. Funct. Mater.* 2012, **22**, 1586-1597.
48. S. Ha, C. Camalier, G. Beck, J. Lee, *Chem. Commun.,* 2009, **20**, 2881-2883.
49. T. Yu, A. Malugin, H. Ghandehari, *ACS Nano*, 2012, **5**, 5717-5728.
50. T. Yu, K. Greish, L. McGill, A. A. Ray, H. Ghandehari, *ACS Nano*, 2012, **6**, 2289-2301.
51. Z. Xu, K. Zhang, C. Hou, D. Wang, X. Liu, X. Guan, X. Zhang, H. Zhang, *J. Mater. Chem. B*, 2014, **2**, 3433-3437.
52. K. N. Yang, C. Q. Zhang, W. Wang, P. C. Wang, J. P. Zhou, X. J. Liang, *Cancer Biol. Med*., 2014,**11**, 34-43.
53. N. S. Kosower, E. M. Kosower, *Int. Rev. Cytol.*, 1978, 54, 109-160.

54. Z. Xu, D. Wang, S. Xu, X. Liu, X. Zhang, H. Zhang, *Chem. Asian J.,* 2014, **9**, 199-205.
55. Y. Wang, M. Shim, N. Levinson, H. Sung, Y. Xia, *Adv. Funct. Mater.*, 2014, **24**, 4206-4220.
56. Y. Liu, L. Feng, T. Liu, L. Zhang, Y. Yao, D. Yu, L. Wang, N. Zhang, *Nanoscale*, 2014, **6**, 3231-3242.
57. H. Wei, R. X. Zhuo, X. Zhang, *Prog. Polym. Sci.*, 2013, **38**, 503-535.
58. N. Ma, Y. Li, H. Xu, Z. Wang, X. Zhang, *J. Am. Chem. Soc.*, 2010, **132**, 442-443.
59. H. Xu, W. Cao, X. Zhang, *Acc. Chem. Res.,* 2013, **46**, 1647-1658.
60. W. Cao, Y. Gu, M. Meineck, T. Li, H. Xu, *J. Am. Chem. Soc.,* 2014, **136**, 5132-5137.
61. W. Stöber, A. Fink, E. Bohn, *J. Colloid Interface Sci.*, 1968, **26**, 62-69.
62. V. Venditto, E. E. Simanek, Mol. Pharm., 2010, **7**, 307-349.
63. P. Gou, W. Liu, W. Mao, J. Tang, Y. Shen, M. Sui, *J. Mater. Chem. B*, 2013, **1**, 284-292.
64. L. Tang, X. Yang, Q. Yin, K. Cai, H. Wang, I. Chaudhury, C. Yao, Q. Zhou, M. Kwon, J. Hartman, I. Dobrucki, L. Dobrucki, L. Borst, S. Lezmi, W. Helferich, A. Ferguson, T. Fan, J. Cheng, *Proc. Natl. Acad. Sci. USA*, 2014, **111**, 15344-15349.
65. C. Ju, R. Mo, J. Xue, L. Zhang, Z. Zhao, L. Xue, Q. Ping, C. Zhang, *Angew. Chem. Int. Ed.,* 2014, **53**, 6253-6258.
66. M. Lee, J. Kim, J. Han, S. Bhuniya, J. Sessler, C. Kang, J. Kim, *J. Am. Chem. Soc*., 2012, **134**, 12668-12674.
67. M. Lee, J. Han, P. Kwon, S. Bhuniya, J. Kim, J. Sessler, C. Kang, J. Kim, *J. Am. Chem. Soc.*, 2012, **134**, 1316-1322.
68. T. C. Chou, *Cancer Res.*, 2010, **70**, 440-446.
69. F. Huang, M. You, T. Chen, G. Zhu, H. Liang, W. Tan, *Chem. Commun.*, 2014, **50**, 3103-3105.
70. P. Huang, D. Wang, Y. Su, W. Huang, Y. Zhou, D. Cui, X. Zhu, D. Yan, *J. Am. Chem. Soc.*, 2014, **136**, 11748-11756.
71. Y. Shen, E. Jin, B. Zhang, C. J. Murphy, M. Sui, J. Zhao, J. Wang, J. Tang, M. Fan, E. V. Kirk, W. J. Murdoch, *J. Am. Chem. Soc.*, 2010, **132**, 4259-4256.
72. Y. Chang, K. Yang, P. Wei, S. Huang, Y. Pei, W. Zhao, Z. Pei, *Angew. Chem. Int. Ed.*, 2014, **53**, 13126-13130.
73. L. Liao, J. Liu, E. C. Dreaden, S. W. Morton, K. E. Shopsowitz, P. T. Hammond, J. A. Johnson, *J. Am. Chem. Soc.,* 2014, **136**, 5896-5899.
74. L. Ma, M. Kohli, A. Smith, *ACS Nano*, 2013, **7**, 9518-9525.